Published in final edited form as:

Neurobiol Aging. 2020 January ; 85: 131–139. doi:10.1016/j.neurobiolaging.2019.10.003.

Adult brain aging investigated using BMC-mcDESPOT based myelin water fraction imaging

Mustapha Bouhrara[†,*,1], **Abinand C. Rejimon**[†,1], **Luis E. Cortina**[1], **Nikkita Khattar**[1], **Christopher M. Bergeron**[1], **Luigi Ferrucci**[2], **Susan M. Resnick**[3], **Richard G. Spencer**[1]

[1]-Laboratory of Clinical Investigation, National Institute on Aging, National Institutes of Health, Baltimore, 21224 MD, USA.

[2]-Translational Gerontology Branch, National Institute on Aging, National Institutes of Health, Baltimore, 21224 MD, USA.

[3]-Laboratory of Behavioral Neuroscience, National Institute on Aging, National Institutes of Health, Baltimore, 21224 MD, USA.

Abstract

The relationship between regional brain myelination and aging has been the subject of intense study, with magnetic resonance imaging (MRI) perhaps the most effective modality for elucidating this. However, most of these studies have used nonspecific methods to probe myelin content, including diffusion tensor imaging, magnetization transfer ratio, and relaxation times. In the current study, we used the BMC-mcDESPOT analysis, a direct and specific method for imaging of myelin water fraction (MWF), a surrogate of myelin content. We investigated age-related differences in MWF in several brain regions in a large cohort of cognitively unimpaired participants, spanning a wide age range. Our results indicate a quadratic, inverted U-shape, relationship between MWF and age in all brain regions investigated, suggesting that myelination continues until middle age followed by decreases at older ages. We also observed that these age-related differences vary across different brain regions, as expected. Our results provide evidence for nonlinear associations between age and myelin in a large sample of well characterized adults, using a direct myelin content imaging method.

Keywords

Myelin water fraction; normal aging; quantitative MRI; BMC-mcDESPOT

[*]**Corresponding author**: Mustapha Bouhrara, *PhD.*, National Institutes of Health (NIH), National Institute on Aging (NIA), Intramural Research Program, BRC 04B-117, 251 Bayview Boulevard, Baltimore, MD 21224, USA. Tel: 410-558-8541, bouhraram@mail.nih.gov.
[†]Equal contribution

Declarations of interest: None

1. INTRODUCTION

Age is the main risk factor for degenerative central nervous system (CNS) disease and associated cognitive and functional impairment. It is therefore crucial to characterize microstructural changes in the brain that occur with normal aging to distinguish them from changes caused by disease. Postmortem studies have shown that myelin degeneration is among the main sequelae of aging and may be associated with concomitant motor and cognitive decline, as well as likely being closely linked to a number of age-associated neurodegenerative disorders and dementias (Bronge et al., 2002; Flynn et al., 2003; Kolasinski et al., 2012). Myelin, an electrical insulator essential for action potential conduction and for transporting trophic support to the neuronal axons of the CNS, is crucial to higher-order integrative functions of the brain. However, the oligodendrocytes that produce myelin and myelin itself are vulnerable to various insults including amyloid-beta and tau protein aggregation and iron accumulation (Bradl and Lassmann, 2010; Nasrabady et al., 2018; Ward et al., 2014). Aside from potential direct damage, these insults can lead to loss of oligodendrocytes or impairment of their myelin synthetic capacity, resulting in deficits in myelin maintenance and repair during turnover, or frank demyelination (Bradl and Lassmann, 2010; Domingues et al., 2016).

It has been observed that brain myelination follows an inverted U-shaped trajectory peaking in the fourth decade of life (Bartzokis et al., 2010). While this nonlinear pattern has been identified in several studies using magnetic resonance imaging (MRI) measures, mostly using diffusion tensor imaging (DTI) and, to a lesser extent, relaxation times imaging, other studies have indicated a linear decrease in myelin from young adulthood to older age using the same MRI modalities (Arshad et al., 2016; Bartzokis et al., 2003; Fjell et al., 2009; Inano et al., 2011; Sullivan and Pfefferbaum, 2006; Yeatman et al., 2014). One possible cause of this discrepancy may be that while DTI outcomes, such as fractional anisotropy (FA) and radial diffusivity, as well as relaxation times and magnetization transfer ratio (MTR), are sensitive to myelin content and therefore provide precise and reliable quantitative metrics, they cannot serve as specific markers of myelination (Alexander et al., 2007; Deoni, 2010). This is due to their sensitivity to a number of tissue properties, including hydration, macromolecular content, axonal density, and architectural features such as fiber crossing and fanning. To address these limitations, more advanced analysis methods based on multicomponent signal decomposition have been introduced to improve both sensitivity and specificity of MR-based myelination studies. Towards this, Mackay and colleagues (MacKay et al., 1994; MacKay and Laule, 2016) pioneered *in-vivo* MR imaging of myelin water fraction (MWF), which has been histologically validated as a proxy for myelin content (Laule et al., 2008; Laule et al., 2006). This approach has been extensively applied to characterize CNS demyelinating diseases and brain development (Borich et al., 2013; Bouhrara et al., 2018a; Dean et al., 2017; Flynn et al., 2003; Laule et al., 2004; Sirrs et al., 2007). Although these methods, like DTI, relaxation time mapping, and MTR provide results that are model-dependent, MWF is, in principle, proportional to myelin content and so provides unique insight into local myelination. However, this method also exhibits greater noise sensitivity than other approaches, leading to ongoing methodological development.

In recent work, Arshad and colleagues found that MWF over the age range of 18 to 84 years follows an inverted U-shaped trend with normative aging across different brain regions (Arshad et al., 2016), indicating brain maturation until middle age, followed by a gradual process of demyelination. We believe this to be the first report investigating age-related differences in MWF in adults' brain spanning a relatively large age range. However, using a similar MRI approach and age range, Faizy and colleagues instead found a linear reduction in MWF with advancing age in all brain regions studied (Faizy et al., 2018). In addition to differences in experimental details, this discrepancy is likely further amplified by the limited cohort sizes in both studies ($n = 61$ and $n = 45$, respectively), as well as the high sensitivity to noise of the multicomponent relaxometry analysis method used (Bouhrara et al., 2018b; Levesque et al., 2010).

In the current study, we investigated the pattern of myelin changes with normative aging in a larger cohort of well-characterized cognitively unimpaired participants ($n = 106$), across the extended age range of 22 to 94 years. Our measures of MWF were conducted using the Bayesian Monte Carlo analysis of multi-component driven equilibrium single-component observation of T_1 and T_2 (BMC-mcDESPOT) method (Bouhrara and Spencer, 2016, 2017). BMC-mcDESPOT generates a high-resolution whole brain MWF map with higher accuracy and precision as compared to conventional MWF analysis methods, and has been previously applied to provide evidence of myelin loss in mild cognitive impairment and dementia using MWF imaging (Bouhrara et al., 2018a). Our main goal in the present work is to use this method to characterize age-related differences in regional brain myelination and to provide further insights into regional brain maturation and aging over the adult lifespan.

2. MATERIAL & METHODS

2.1. Participants

Participants were drawn from two ongoing healthy aging cohorts at the National Institute on Aging (NIA). Ninety volunteers recruited from the Baltimore Longitudinal Study of Aging (BLSA) (Ferrucci, 2008; Shock, 1985), and thirty-five from the Genetic and Epigenetic Signatures of Translational Aging Laboratory Testing (GESTALT) were enrolled in this study. The study populations, experimental design, and measurement protocols of the BLSA have been previously reported (Ferrucci, 2008; Shock, 1985). The BLSA is a longitudinal cohort study funded and conducted by the NIA Intramural Research Program (IRP). Established in 1958, the BLSA enrolls community-dwelling adults with no major chronic conditions or functional impairments. The GESTALT study is also a study of healthy volunteers, initiated in 2015, and funded and conducted by the NIA IRP. The goal of the BLSA and GESTALT studies is to evaluate multiple biomarkers related to aging. We note that the inclusion and exclusion criteria for these two studies are essentially identical. Participants underwent testing at the National Institute on Aging's clinical research unit and were excluded if they had metallic implants, or neurologic, medical, or psychiatric disorders. All participants underwent a Mini Mental State Examination (MMSE) (Table 1) and thirteen cognitively impaired participants were excluded. The final cohort consisted of 106 cognitively unimpaired volunteers ranging in age from 22 to 94 years (mean ± standard deviation 55.1 ± 21.3 years) of which 58 were men (56.7 ± 22.5 years) and 48 were women

(53.4 ± 20 years), after removal of six imaging datasets with technically limited scans, caused by, for example, excessive motion. Figure 1 provides a detailed distribution of the number of participants per age-decade and for each sex. Age, MMSE, and years of education did not differ significantly between men and women (Table 1). Experimental procedures were performed in compliance with our local Institutional Review Board, and participants provided written informed consent.

2.2. Data acquisition

MRI scans were performed using a 3T Philips MRI system (Achieva, Best, The Netherlands). For each participant, 3D spoiled gradient recalled echo (SPGR) images were acquired with flip angles (FAs) of [2 4 6 8 10 12 14 16 18 20]°, echo time (TE) of 1.37 ms, repetition time (TR) of ~5 ms, and acquisition time of 5 min, as well as 3D balanced steady state free precession (bSSFP) images acquired with FAs of [2 7 11 16 24 32 40 60]°, TE of 2.8 ms, TR of 5.8 ms, and acquisition time of ~6 min. The bSSFP images were acquired with radiofrequency excitation pulse phase increments of 0 or π in order to account for off-resonance effects (Deoni, 2011). All SPGR and bSSFP images were acquired with an acquisition matrix of 150 × 130 × 94, voxel size of 1.6 mm × 1.6 mm × 1.6 mm, without signal averaging. Further, we used the double-angle method to correct for excitation radio frequency inhomogeneity (Stollberger and Wach, 1996). For that, two fast spin-echo images were acquired with flip angles of 45° and 90°, echo time of 102 ms, repetition time of 3000 ms, acquisition voxel size of 2.6 mm × 2.6 mm × 4 mm, and acquisition time of ~4 min. The total acquisition time for the entire imaging protocol was ~21 min.

All images were obtained with field of view of 240 mm × 208 mm × 150 mm and reconstructed to a voxel size of 1 mm × 1 mm × 1 mm. We emphasize that all MRI studies and ancillary measurements were performed with the same MRI system, running the same pulse sequences, at the same facility, and directed by the same investigators for both BLSA and GESTALT participants.

2.3. Data processing

After thorough visual inspection of data quality for each participant, the scalp, ventricles, and other nonparenchymal regions within the images were eliminated using the FMRIB Software Library (FSL) using an input image consisting of the SPGR images averaged over all 10 flip angles (Jenkinson et al., 2012); this provides high tissue contrast and signal-to-noise ratio for accurate segmentation. Next, a whole-brain MWF map was generated for the remaining regions of interest using the BMC-mcDESPOT analysis (Bouhrara and Spencer, 2016, 2017). Briefly, BMC-mcDESPOT assumes a two-component non-exchanging system consisting of a short and long T_1 and T_2 components. The short component corresponds to the signal of water trapped within the myelin sheets while the long component corresponds to intra/extra cellular water. Analysis was performed explicitly accounting for nonzero TE as incorporated into the TE-corrected-mcDESPOT signal model (Bouhrara and Spencer, 2015). BMC-mcDESPOT permits determination of MWF in each voxel through marginalization over nuisance parameters, that is, relaxation times. This is in contrast to conventional stochastic region contraction algorithm evaluating single parameters combinations for a joint estimation of all parameters to optimize the objective function; this leads to potential

difficulties with local minima, especially in higher-dimensional problems such as mcDESPOT (Bouhrara and Spencer, 2017; West et al., 2019). However, high-dimensional integration is needed in BMC-mcDESPOT to perform the marginalization which is computationally extensive; this is overcome using Monte Carlo sampling. The averaged SPGR image of each participant was registered using nonlinear registration to the MNI standard space image using the FSL software tools FLIRT and FNIRT. The derived transformation matrix was then applied to the MWF map for that corresponding participant. Twenty five regions of interest (ROIs) were defined encompassing white matter (WM) and deep gray matter (GM) regions of the brain corresponding to regions previously identified as the focus of investigation (Arshad et al., 2016; Faizy et al., 2018; Uddin et al., 2019) (Figure 2). Twenty one WM ROIs were derived from the MNI structural atlas, corresponding to whole brain (WB) WM, frontal lobes (FL), parietal lobe (PL), occipital lobe (OL), temporal lobe (TL), cerebellum (CRB), splenium of corpus callosum (SCC), body of corpus callosum (BCC), genu of corpus callosum (GCC), and internal capsule (IC), anterior corona radiata (ACR), posterior corona radiata (PCR), cerebral peduncle (CP), posterior thalamic radiation (PTR), anterior thalamic radiation (ATR), superior fronto-occipital fasciculus (SFOF), inferior fronto-occipital fasciculus (IFOF), superior longitudinal fasciculus (SLF), inferior longitudinal fasciculus (ILF), forceps major (FM), forceps minor (Fm), while the four deep GM regions, corresponding to insula (Ins), caudate (Cau), putamen (Put), and thalamus (Tha), were derived from the Johns Hopkins University (JHU) ICM-DTI-81 atlas. For the WM regions, we used the FSL tool FAST to delineate the amount of WM in each voxel and included only voxels displaying more than 80% WM. Finally, for each ROI and each participant, mean MWF values were calculated. All analyses, including MWF map calculation, registration, and ROI segmentation, were performed blinded to any information related to participants age, sex, and cognitive status.

2.4. Statistical analysis

For each ROI, the effects of age and sex on myelination were investigated using linear regression with the mean MWF within the ROI as the dependent variable and sex, age, and age^2 as independent variables after mean age centering. The initial model incorporated interactions between sex and age as well as sex and age^2, but any term was removed if found not to be significant. The resulting parsimonious model was then constructed without the nonsignificant interactions. In all cases, the threshold for statistical significance was $p < 0.05$ after correction for multiple ROI comparisons using the false discovery rate (FDR) method (Benjamini, 2010). Furthermore, for each ROI, we performed a runs test for randomness on the fit residuals for the regression models with and without a quadratic age term. Finally, for each of the 25 brain regions, ANOVA statistical analysis was performed to test for differences between mean MWF values averaged over participants within 10-year intervals; these age intervals are given in Fig. 3. Post-hoc Bonferroni correction was applied at the significance level of 0.002 (*i.e.* 0.05/25) to account for multiple comparisons. All calculations were performed with MATLAB (MathWorks, Natick, MA, USA).

3. RESULTS

Figure 3 shows average MWF maps by age decade over the adult lifespan for three representative axial slices. Visual inspection indicated increases in MWF values from early adulthood until middle age (*i.e.* 40–49 years), followed by reduced MWF in several brain regions, consistent with progressive myelination followed by reductions in myelin. Furthermore, we note that different regions exhibit different pattern associations between MWF and age, with the occipital and parietal lobes exhibiting greater MWF values as compared to the more anterior brain regions.

Figure 4 shows quantitative results for MWF values from all participants as a function of age for the indicated 21 WM regions and 4 deep GM regions. Visual inspection shows increasing MWF until middle age followed by decreases in MWF with age in all examined ROIs, in agreement with Figure 3. The best-fit curves indicate that while the fundamental U-shaped relationship between MWF and age was consistent across all ROIs, the age curves displayed regional variation. Furthermore, in agreement with Figure 3, the high MWF values were found in the occipital and parietal lobes, with the frontal and temporal lobes exhibiting overall lower MWF values. Overall, all WM regions exhibited high MWF values while the lowest MWF values were found in the deep GM regions, as expected. In addition, we note that that as compared to the other regions evaluated, caudate and putamen regions exhibited much lower R^2 values for the correlation between MWF and age. Finally, the R^2 values of the model fit incorporating a quadratic age term were higher than the R^2 values of the model fit incorporating a linear age term only, for all ROIs (Table 1 of supplementary material).

Significant age effects were found for all brain regions evaluated except the caudate after FDR correction and the forceps major before FDR correction (Table 2). Similarly, the quadratic effect of age, age^2, was significant in all brain regions except in the genu of the corpus callosum, the cerebral peduncle, and the anterior thalamic radiation (Table 2). Our statistical analyses indicate that all ROIs exhibited non-significant interactions between age^2 and sex. However, while there were significant main effects of sex in three brain regions, namely the parietal lobes ($F = 4.0$, $p = 0.048$), the body of corpus callosum ($F = 5.2$, $p = 0.025$), and the splenium of corpus callosum ($F = 7.3$, $p = 0.008$), significance did not survive FDR correction. In these brain regions, women had ~10% higher myelin content than men. Interaction between age and sex was also nominally significant in five brain regions, but in these cases as well significance did not survive the FDR correction; these regions were the whole brain ($F = 4.45$, $p = 0.04$), the temporal lobes ($F = 4.3$, $p = 0.041$), the body of corpus callosum ($F = 5.1$, $p = 0.026$), the anterior corona radiata ($F = 5.8$, $p = 0.018$), and the posterior corona radiata ($F = 10.7$, $p = 0.002$). In these regions, women showed a non-significant trend to greater reduction in MWF with age as compared to men.

To further support our choices of model, we applied the runs test of randomness (RTR) to the residuals from the parsimonious model fit to determine whether the residuals were randomly distributed. For all ROIs, the RTR test indicated randomness ($p > 0.05$ for structured residuals), showing that the model provided an adequate fit to the data, except for the posterior corona radiata, anterior thalamic radiation, and the forceps major and minor. We note that except for the forceps minor, the anterior corona radiata, the inferior

longitudinal fasciculus, and the genu of corpus callosum, all other ROIs exhibited lower RTR significance of the model incorporating the quadratic age term as compared to that incorporating the age term only; this further supports the choice of the quadratic regression model. Finally, for each ROI, we determined the specific year at which MWF peaked (Fig. 4). As seen, white matter regions overall peaked earlier as compared to deep gray matter regions, in which fully developed myelination may serve a less central role in function. For the WM regions, the MWF of the occipital lobes, temporal lobes, and cerebellum reached a maximum at later ages as compared to all other WM structures.

Finally, the ANOVA analysis comparing the regional mean MWF values averaged over participants within 10-year age intervals indicated that for all ROIs except the cerebral peduncles, the forceps major, and the caudate, there was a statistically significant variation in MWF values across age (Table 2). However, the cerebellum, the genu of corpus callosum, the inferior front-occipital fasciculus, the inferior longitudinal fasciculus, the forceps minor, and the putamen regions did not survive Bonferroni correction (Fig. 1 of the supplementary material). The post hoc analysis indicated that significance was mainly between age-intervals 20–29, 30–39, or 40–49 and 60–69, 70–79 or 80–89. Figure 1 of the supplementary material provides a detailed description of these differences.

4. DISCUSSION

Myelin water fraction (MWF) provides important insights for understanding brain maturation and neurodegeneration (MacKay and Laule, 2016). However, to our knowledge, only two *in-vivo* studies have been conducted to date to investigate the regional associations between myelin and aging in cognitively normal adults (Arshad et al., 2016; Faizy et al., 2018). Our work has several advantages with regard to these previous MWF studies. We made use of a larger cohort spanning a wider age range and with relatively dense sampling for each decade of life. Moreover, we employed a highly stabilized technique for MWF mapping, enabling us to derive MWF maps at higher-spatial resolution (Fig. 3), leading to better delineation of small brain structures and decreased partial volume effects, in which measurements of a given brain region are contaminated by adjacent regions.

Our results indicate a quadratic association between MWF and age in most white matter and deep gray matter regions (Figs. 3–4). These results are consistent with Arshad and colleagues' recent study indicating an inverted U-shape trend of MWF values with age in different white matter regions (Arshad et al., 2016). The quadratic association between MWF and age is attributed to the process of myelination from youth through middle age, followed by demyelination in later years (Arshad et al., 2016; Bartzokis et al., 2010); this pattern is in agreement with postmortem observations (Peters, 2002; Tang et al., 1997). As expected, we found that different regions exhibit both similarities and differences in associations between MWF and age, with most regions peaking at the fourth life decade. This finding is in good agreement with several studies based on myelin-sensitive, but nonspecific, MRI methods such as diffusion tensor imaging and relaxation times (Bartzokis et al., 2010; Okubo et al., 2017; Westlye et al., 2010; Yeatman et al., 2014). Our results also showed relatively high myelin content in the cerebral peduncle, thalamic radiation, corona radiata, and superior longitudinal fasciculus (Fig. 4 and Table 2 of supplementary material),

in agreement with Uddin's and colleagues and Arshad's and colleagues studies (Arshad et al., 2016; Uddin et al., 2019), indicating the sensitivity of MWF imaging to these particular complex fiber regions. Moreover, parameter maps (Fig. 3) and quantitative analyses (Fig. 4 and Table 2) showed that the occipital lobes exhibited delayed demyelination as compared to the other lobes. This pattern is consistent with the retrogenesis hypothesis (first in-last out), in which posterior brain regions are spared from degeneration as compared to anterior brain regions (Bender et al., 2016; Brickman et al., 2012; Raz, 2000; Stricker et al., 2009). However, additional studies, and in particular longitudinal studies, are required for further validation of this finding. Moreover, iron-rich structures such as the caudate and putamen exhibited very low R^2 values (Fig. 4); this is likely due to various biological or post-processing factors. Indeed, studies have shown that these regions are particularly susceptible to increased iron deposition during the processes of normative aging (Pfefferbaum et al., 2009; Wang et al., 2012). This iron may serve to catalyze free radical reactions promoting lipid peroxidation and oxidative tissue damage, promoting myelin breakdown and consequent additional release of iron. Given the strong influence of iron on transverse relaxation, small variations in this process would be expected to lead to relatively large variations in MWF, limiting the strength of correlations. This indicates the importance of linking MWF analysis with methods such as quantitative susceptibility mapping in subsequent studies. Further, accurate segmentation of these regions is challenging, mainly due to their small size as well as relatively poor contrast between adjacent substructures. While we have conducted a careful examination of all ROIs, some degree of partial volume bias in the calculated MWF values cannot be excluded.

Of note, Arshad and colleagues found that myelin content peaks around the fourth to sixth decade of life in contrast to our results, which indicated somewhat earlier peak myelination. This partial discrepancy is likely due to several differences between the current study and their study including their more limited cohort size and age range, less homogeneous sampling density, and the noise-sensitive and low-resolution MWF mapping methods used in their investigation. As an illustration, we performed a linear regression on a subset of our datasets covering the age range used in (Arshad et al., 2016), that is, excluding participants over 75 years of age. The results clearly indicate a shift of the apparent MWF peak, derived from the fit, towards later ages; this may partially explain the observations of the aforementioned study (Fig. 5) (Fjell et al., 2010). Another potential source of the discrepancy in the literature regarding the apparent age of maximum myelination is the dependency on the variables used in the final regression model; with these differences, the discrepancy may be due to modeling rather than physiologic differences.

Overall, it must be recognized that the relative importance of the linear versus quadratic age trends, as well as apparent ages of maximal myelination, and the specific values of the parameters and their significant, will exhibit some variability as a function of sampling density within age groups, range of ages incorporated, and consistency of data. In addition, the choice of a quadratic regression model is conventional and consistent with our visual inspection and well-represented in the literature. Thus, this choice must be regarded as an expedient to model the data, without representing this as a description of underlying physiologic processes. Other models, such as piecewise linear may serve equally well as data descriptors. However, the present analysis provides a basic demonstration of

myelination trajectories as increasing from early adulthood through middle age, with a decrease thereafter. Finally, derived MWF values and their association with age are strongly influenced by iron, which is well-known to accumulate in several brain regions with increasing age (Hallgren and Sourander, 1958). It has been shown that diffusion of iron into the extracellular space may shorten the corresponding transverse relaxation time leading to an artificial overestimation of MWF values (Birkl et al., 2019). Therefore, the effect of iron could also explain reported differences in the age-dependence of myelination, since all imaging methods exhibit some sensitivity to transverse relaxation.

Our analysis was conducted in several brain regions. This was made possible by our application of a particularly high-resolution MWF imaging method as compared to conventional methods (Bouhrara and Spencer, 2017). In fact, the mcDESPOT approach pioneered by Deoni and colleagues (Deoni et al., 2008) permits rapid imaging MWF mapping, and has been extensively used to characterize brain maturation in pediatric participants as well as myelination changes in various neurodegenerative diseases (Bouhrara et al., 2018a; Dean et al., 2017; Dean et al., 2015; Deoni et al., 2015). However, parameter estimates using mcDESPOT can show a great deal of variability with respect to noise (Bouhrara et al., 2015; Lankford and Does, 2013; West et al., 2019). Our Bayesian implementation greatly stabilizes these parameter estimates, thereby permitting high-spatial resolution imaging with greatly improved parameter estimates (Bouhrara and Spencer, 2016, 2017). This advance was critical to accurately delineate small brain structures, such as the deep gray matter regions and various white matter structures, while greatly minimizing partial volume bias; this represents one of the main limitations of conventional mcDESPOT methods as well as multi-echo-based techniques (Alonso-Ortiz et al., 2015). The use of BMC-mcDESPOT could be particularly suitable for studies focusing on small brain structures, such as brainstem substructures, or for whole brain coverage with high spatial resolution.

We found statistically significant sex differences in a limited number of brain regions before FDR correction, with women exhibiting higher myelin content than men. This finding is in good agreement with the literature (Arshad et al., 2016). We also found that the MWF in women, compared with men, shows greater reduction with age in several brain regions, although these observations were not significant after FDR correction. These trends indicate potential lines of investigation in larger cohorts, with the current study potentially underpowered to detect subtle group differences. Indeed, the sex differences we observed in myelin are consistent with previous demonstrations that proliferation of oligodendrocytes and myelin proteins are regulated differently in males and females (Cerghet et al., 2006; Greer et al., 2004). A recent study suggests that sex steroids may influence this differential regulation, possibly contributing to sex differences in repair (Marin-Husstege et al., 2004). Cross-sectional and longitudinal studies indicate sex differences in brain maturational processes and emphasize the importance of myelination in understanding the mechanism of neuropsychiatric disorders. Finally, the age/sex interaction was significant in a limited number of brain regions before FDR correction; this is unlikely to be due to differences in sex distribution within this cohort, since such differences were minimal (Fig. 1).

Our calculated MWF mean values were overall in good agreement with those previously reported (Dean et al., 2017; Dvorak et al., 2019). However, we note that mcDESPOT in general, and BMC-mcDESPOT in particular, provide relatively higher MWF values as compared to MSE-based methods. This discrepancy is likely due several physiologic and experimental factors that are not modeled in either mcDESPOT- or MSE-based signal formalisms, including exchange between water pools (Harkins et al., 2012; van Gelderen and Duyn, 2019). However, incorporation of water exchange in conventional mcDESPOT signal modeling leads to a further increase in the instability of MWF determinations (Bouhrara et al., 2015; Lankford and Does, 2013; West et al., 2019). We are currently investigating the potential of BMC-mcDESPOT analysis to improve MWF determination when water exchange is incorporated. Other parameters that may bias MWF estimation are magnetization transfer between free water protons and macromolecules, T_1 effects resulting from short TRs, off-resonance effects, J-coupling, spin locking, internal gradients, and signal attenuation due to differences in water diffusion in within different compartments. These issues remain as major challenges throughout quantitative MR studies of myelin, with significant ongoing activity seeking to either improve existing methods or to introduce new techniques for accurate MWF determination.

Although our work examines a large cohort using advanced methodology, certain limitations remain. While our cohort spanned a wide age range, it does not include very young participants (< 20 years old); this limitation derives from the exclusion criteria of the BLSA and GESTALT studies. Inclusion of younger participants may influence the shape of MWF age-related trajectories (Fjell et al., 2010). We also note that it was not feasible to obtain optimal uniform sampling across all age intervals in this convenience sample of participants in ongoing research protocols, with the number of subjects aged 50–70 years being lower as compared to the other age decades. This may also influence the overall interpretability of myelination during the process of aging, as discussed above. Nevertheless, we obtained a meaningful sample size across the age range of our study. Finally, our dataset is cross-sectional, so that the quadratic trajectories observed here and elsewhere require further validation through longitudinal studies. Such work, motivated by the present results, is underway.

5. CONCLUSIONS

Using an advanced magnetic resonance myelin water fraction mapping technique, we showed that myelin content follows an inverted-U shaped trajectory with normal aging. We interpret this as indicating brain maturation with respect to myelination until middle age followed by decreased myelination with advancing age. These age curves during adulthood vary across different brain regions, as expected based on histologic studies. These results support the overall conclusions of previous MRI studies that implemented sensitive but nonspecific myelin-mapping approaches. Finally, our results provide reference values for MWF values in normative aging.

Supplementary Material

Refer to Web version on PubMed Central for supplementary material.

ACKNOWLEDGEMENT

This work was supported by the Intramural Research Program of the National Institute on Aging of the National Institutes of Health. We gratefully acknowledge Denise Melvin and Linda Zukley for their assistance with participants recruitment and logistics.

7. REFERENCES

Alexander AL, Lee JE, Lazar M, Field AS, 2007 Diffusion tensor imaging of the brain. Neurotherapeutics : the journal of the American Society for Experimental NeuroTherapeutics 4(3), 316329.

Alonso-Ortiz E, Levesque IR, Pike GB, 2015 MRI-based myelin water imaging: A technical review. Magnetic resonance in medicine 73(1), 70–81. [PubMed: 24604728]

Arshad M, Stanley JA, Raz N, 2016 Adult age differences in subcortical myelin content are consistent with protracted myelination and unrelated to diffusion tensor imaging indices. NeuroImage 143, 26–39. [PubMed: 27561713]

Bartzokis G, Cummings JL, Sultzer D, Henderson VW, Nuechterlein KH, Mintz J, 2003 White Matter Structural Integrity in Healthy Aging Adults and Patients With Alzheimer Disease: A Magnetic Resonance Imaging Study. Archives of neurology 60(3), 393–398. [PubMed: 12633151]

Bartzokis G, Lu PH, Tingus K, Mendez MF, Richard A, Peters DG, Oluwadara B, Barrall KA, Finn JP, Villablanca P, Thompson PM, Mintz J, 2010 Lifespan trajectory of myelin integrity and maximum motor speed. Neurobiology of aging 31(9), 1554–1562. [PubMed: 18926601]

Bender AR, Volkle MC, Raz N, 2016 Differential aging of cerebral white matter in middle-aged and older adults: A seven-year follow-up. Neuroimage 125, 74–83. [PubMed: 26481675]

Benjamini Y, 2010 Discovering the false discovery rate. Journal of the Royal Statistical Society. Series B (Statistical Methodology) 72(4), 405–416.

Birkl C, Birkl-Toeglhofer AM, Endmayr V, Hoftberger R, Kasprian G, Krebs C, Haybaeck J, Rauscher A, 2019 The influence of brain iron on myelin water imaging. Neuroimage 199, 545–552. [PubMed: 31108214]

Borich MR, MacKay AL, Vavasour IM, Rauscher A, Boyd LA, 2013 Evaluation of white matter myelin water fraction in chronic stroke. Neuroimage: Clinical 2, 569–580.

Bouhrara M, Reiter D, Bergeron C, Zukley L, Ferrucci L, Resnick S, Spencer R, 2018a Evidence of demyelination in mild cognitive impairment and dementia using a direct and specific magnetic resonance imaging measure of myelin content. Alzheimer's & Dementia 14(8), 998–1004.

Bouhrara M, Reiter DA, Celik H, Fishbein KW, Kijowski R, Spencer RG, 2015 Analysis of mcDESPOT- and CPMG-derived parameter estimates for two-component nonexchanging systems. Magnetic resonance in medicine.

Bouhrara M, Reiter DA, Maring MC, Bonny JM, Spencer RG, 2018b Use of the NESMA Filter to Improve Myelin Water Fraction Mapping with Brain MRI. Journal of neuroimaging : official journal of the American Society of Neuroimaging.

Bouhrara M, Spencer RG, 2015 Incorporation of nonzero echo times in the SPGR and bSSFP signal models used in mcDESPOT. Magnetic resonance in medicine 74(5), 1227–1235. [PubMed: 26407635]

Bouhrara M, Spencer RG, 2016 Improved determination of the myelin water fraction in human brain using magnetic resonance imaging through Bayesian analysis of mcDESPOT. NeuroImage 127, 456–471. [PubMed: 26499810]

Bouhrara M, Spencer RG, 2017 Rapid simultaneous high-resolution mapping of myelin water fraction and relaxation times in human brain using BMC-mcDESPOT. NeuroImage 147, 800–811. [PubMed: 27729276]

Bradl M, Lassmann H, 2010 Oligodendrocytes: biology and pathology. Acta Neuropathologica 119(1), 37–53. [PubMed: 19847447]

Brickman AM, Meier IB, Korgaonkar MS, Provenzano FA, Grieve SM, Siedlecki KL, Wasserman BT, Williams LM, Zimmerman ME, 2012 Testing the white matter retrogenesis hypothesis of cognitive aging. Neurobiology of aging 33(8), 1699–1715. [PubMed: 21783280]

Bronge L, Bogdanovic N, Wahlund LO, 2002 Postmortem MRI and Histopathology of White Matter Changes in Alzheimer Brains. Dementia and geriatric cognitive disorders 13(4), 205–212. [PubMed: 12006730]

Cerghet M, Skoff RP, Bessert D, Zhang Z, Mullins C, Ghandour MS, 2006 Proliferation and death of oligodendrocytes and myelin proteins are differentially regulated in male and female rodents. The Journal of neuroscience : the official journal of the Society for Neuroscience 26(5), 1439–1447. [PubMed: 16452667]

Dean DC 3rd, Hurley SA, Kecskemeti SR, O'Grady JP, Canda C, Davenport-Sis NJ, Carlsson CM, Zetterberg H, Blennow K, Asthana S, Sager MA, Johnson SC, Alexander AL, Bendlin BB, 2017 Association of Amyloid Pathology With Myelin Alteration in Preclinical Alzheimer Disease. JAMA Neurol 74(1), 41–49. [PubMed: 27842175]

Dean DC 3rd, O'Muircheartaigh J, Dirks H, Waskiewicz N, Lehman K, Walker L, Piryatinsky I, Deoni SC, 2015 Estimating the age of healthy infants from quantitative myelin water fraction maps. Human brain mapping 36(4), 1233–1244. [PubMed: 25640476]

Deoni SC, 2010 Quantitative relaxometry of the brain. Topics in magnetic resonance imaging : TMRI 21(2), 101–113. [PubMed: 21613875]

Deoni SC, 2011 Correction of main and transmit magnetic field (B0 and B1) inhomogeneity effects in multicomponent-driven equilibrium single-pulse observation of T1 and T2. Magnetic resonance in medicine 65(4), 1021–1035. [PubMed: 21413066]

Deoni SC, Rutt BK, Arun T, Pierpaoli C, Jones DK, 2008 Gleaning multicomponent T1 and T2 information from steady-state imaging data. Magnetic resonance in medicine 60(6), 1372–1387. [PubMed: 19025904]

Deoni SC, Zinkstok JR, Daly E, Ecker C, Williams SC, Murphy DG, 2015 White-matter relaxation time and myelin water fraction differences in young adults with autism. Psychological medicine 45(4), 795–805. [PubMed: 25111948]

Domingues HS, Portugal CC, Socodato R, Relvas JB, 2016 Oligodendrocyte, Astrocyte, and Microglia Crosstalk in Myelin Development, Damage, and Repair. Frontiers in Cell and Developmental Biology 4(71).

Dvorak A, Liu H, Ljungberg E, Vavasour I, Lee L, MacKay A, Tam R, Li D, Rauscher A, Laule C, Kolind S, 2019 Multivariate template creation of a myelin water brain atlas with GRASE and mcDESPOT, ISMRM Canada.

Faizy TD, Kumar D, Broocks G, Thaler C, Flottmann F, Leischner H, Kutzner D, Hewera S, Dotzauer D, Stellmann J-P, Reddy R, Fiehler J, Sedlacik J, GelliRen S, 2018 Age-Related Measurements of the Myelin Water Fraction derived from 3D multi-echo GRASE reflect Myelin Content of the Cerebral White Matter. Scientific Reports 8(1), 14991. [PubMed: 30301904]

Ferrucci L, 2008 The Baltimore Longitudinal Study of Aging (BLSA): a 50-year-long journey and plans for the future. The journals of gerontology. Series A, Biological sciences and medical sciences 63(12), 14161419.

Fjell AM, Engvig A, Tamnes CK, Grydeland H, Walhovd KB, Westlye LT, 0stby Y, Dale AM, Bj0rnerud A, Due-T0nnessen P, 2009 Life-Span Changes of the Human Brain White Matter: Diffusion Tensor Imaging (DTI) and Volumetry. Cerebral Cortex 20(9), 2055–2068. [PubMed: 20032062]

Fjell AM, Walhovd KB, Westlye LT, Ostby Y, Tamnes CK, Jernigan TL, Gamst A, Dale AM, 2010 When does brain aging accelerate? Dangers of quadratic fits in cross-sectional studies. Neuroimage 50(4), 1376–1383. [PubMed: 20109562]

Flynn SW, Lang DJ, Mackay AL, Goghari V, Vavasour IM, Whittall KP, Smith GN, Arango V, Mann JJ, Dwork AJ, Falkai P, Honer WG, 2003 Abnormalities of myelination in schizophrenia detected in vivo with MRI, and post-mortem with analysis of oligodendrocyte proteins. Molecular psychiatry 8(9), 811–820. [PubMed: 12931208]

Greer JM, Csurhes PA, Pender MP, McCombe PA, 2004 Effect of gender on T-cell proliferative responses to myelin proteolipid protein antigens in patients with multiple sclerosis and controls. Journal of Autoimmunity 22(4), 345–352. [PubMed: 15120759]

Hallgren B, Sourander P, 1958 The effect of age on the non-haemin iron in the human brain. Journal of neurochemistry 3(1), 41–51. [PubMed: 13611557]

Harkins KD, Dula AN, Does MD, 2012 Effect of intercompartmental water exchange on the apparent myelin water fraction in multiexponential T2 measurements of rat spinal cord. Magnetic resonance in medicine 67(3), 793–800. [PubMed: 21713984]

Inano S, Takao H, Hayashi N, Abe O, Ohtomo K, 2011 Effects of age and gender on white matter integrity. AJNR. American journal of neuroradiology 32(11), 2103–2109. [PubMed: 21998104]

Jenkinson M, Beckmann CF, Behrens TE, Woolrich MW, Smith SM, 2012 FSL. Neuroimage 62(2), 782–790. [PubMed: 21979382]

Kolasinski J, Stagg CJ, Chance SA, Deluca GC, Esiri MM, Chang E-H, Palace JA, McNab JA, Jenkinson M, Miller KL, Johansen-Berg H, 2012 A combined post-mortem magnetic resonance imaging and quantitative histological study of multiple sclerosis pathology. Brain : a journal of neurology 135(Pt 10), 2938–2951. [PubMed: 23065787]

Lankford CL, Does MD, 2013 On the inherent precision of mcDESPOT. Magnetic resonance in medicine 69(1), 127–136. [PubMed: 22411784]

Laule C, Kozlowski P, Leung E, Li DK, Mackay AL, Moore GR, 2008 Myelin water imaging of multiple sclerosis at 7 T: correlations with histopathology. NeuroImage 40(4), 1575–1580. [PubMed: 18321730]

Laule C, Leung E, Lis DK, Traboulsee AL, Paty DW, MacKay AL, Moore GR, 2006 Myelin water imaging in multiple sclerosis: quantitative correlations with histopathology. Multiple sclerosis (Houndmills, Basingstoke, England) 12(6), 747–753.

Laule C, Vavasour IM, Moore GR, Oger J, Li DK, Paty DW, MacKay AL, 2004 Water content and myelin water fraction in multiple sclerosis. A T2 relaxation study. Journal of neurology 251(3), 284–293. [PubMed: 15015007]

Levesque IR, Chia CL, Pike GB, 2010 Reproducibility of in vivo magnetic resonance imaging-based measurement of myelin water. Journal of magnetic resonance imaging : JMRI 32(1), 60–68. [PubMed: 20578011]

MacKay A, Whittall K, Adler J, Li D, Paty D, Graeb D, 1994 In vivo visualization of myelin water in brain by magnetic resonance. Magnetic resonance in medicine 31(6), 673–677. [PubMed: 8057820]

MacKay AL, Laule C, 2016 Magnetic Resonance of Myelin Water: An in vivo Marker for Myelin. Brain Plasticity 2(1), 71–91. [PubMed: 29765849]

Marin-Husstege M, Muggironi M, Raban D, Skoff RP, Casaccia-Bonnefil P, 2004 Oligodendrocyte Progenitor Proliferation and Maturation Is Differentially Regulated by Male and Female Sex Steroid Hormones. Developmental Neuroscience 26(2–4), 245–254. [PubMed: 15711064]

Nasrabady SE, Rizvi B, Goldman JE, Brickman AM, 2018 White matter changes in Alzheimer's disease: a focus on myelin and oligodendrocytes. Acta Neuropathologica Communications 6, 22. [PubMed: 29499767]

Okubo G, Okada T, Yamamoto A, Fushimi Y, Okada T, Murata K, Togashi K, 2017 Relationship between aging and T1 relaxation time in deep gray matter: A voxel-based analysis. Journal of magnetic resonance imaging : JMRI 46(3), 724–731. [PubMed: 28152255]

Peters A, 2002 The effects of normal aging on myelin and nerve fibers: a review. Journal of neurocytology 31(8–9), 581–593. [PubMed: 14501200]

Pfefferbaum A, Adalsteinsson E, Rohlfing T, Sullivan EV, 2009 MRI estimates of brain iron concentration in normal aging: comparison of field-dependent (FDRI) and phase (SWI) methods. NeuroImage 47(2), 493–500. [PubMed: 19442747]

Raz N, 2000 Aging of the brain and its impact on cognitive performance: Integration of structural and functional findings, The handbook of aging and cognition, 2nd ed. Lawrence Erlbaum Associates Publishers, Mahwah, NJ, US, pp. 1–90.

Shock N, 1985 Normal Human Aging: The Baltimore Longitudinal Study of Aging. Journal of Gerontology 40(6), 767–767.

Sirrs SM, Laule C, Madler B, Brief EE, Tahir SA, Bishop C, MacKay AL, 2007 Normal-appearing white matter in patients with phenylketonuria: water content, myelin water fraction, and metabolite concentrations. Radiology 242(1), 236–243. [PubMed: 17185670]

Stollberger R, Wach P, 1996 Imaging of the active B1 field in vivo. Magnetic resonance in medicine 35(2), 246–251. [PubMed: 8622590]

Stricker NH, Schweinsburg BC, Delano-Wood L, Wierenga CE, Bangen KJ, Haaland KY, Frank LR, Salmon DP, Bondi MW, 2009 Decreased white matter integrity in late-myelinating fiber pathways in Alzheimer's disease supports retrogenesis. NeuroImage 45(1), 10–16. [PubMed: 19100839]

Sullivan EV, Pfefferbaum A, 2006 Diffusion tensor imaging and aging. Neuroscience & Biobehavioral Reviews 30(6), 749–761. [PubMed: 16887187]

Tang Y, Nyengaard JR, Pakkenberg B, Gundersen HJ, 1997 Age-induced white matter changes in the human brain: a stereological investigation. Neurobiology of aging 18(6), 609–615. [PubMed: 9461058]

Uddin MN, Figley TD, Solar KG, Shatil AS, Figley CR, 2019 Comparisons between multi-component myelin water fraction, T1w/T2w ratio, and diffusion tensor imaging measures in healthy human brain structures. Scientific Reports 9(1), 2500. [PubMed: 30792440]

van Gelderen P, Duyn JH, 2019 White matter intercompartmental water exchange rates determined from detailed modeling of the myelin sheath. Magnetic resonance in medicine 81(1), 628–638. [PubMed: 30230605]

Wang D, Li W-B, Wei X-E, Li Y-H, Dai Y-M, 2012 An Investigation of Age-Related Iron Deposition Using Susceptibility Weighted Imaging. PloS one 7(11), e50706. [PubMed: 23226360]

Ward RJ, Zucca FA, Duyn JH, Crichton RR, Zecca L, 2014 The role of iron in brain ageing and neurodegenerative disorders. The Lancet. Neurology 13(10), 1045–1060. [PubMed: 25231526]

West DJ, Teixeira RPAG, Wood TC, Hajnal JV, Tournier J-D, Malik SJ, 2019 Inherent and unpredictable bias in multi-component DESPOT myelin water fraction estimation. NeuroImage 195, 78–88. [PubMed: 30930311]

Westlye LT, Walhovd KB, Dale AM, Bjornerud A, Due-Tonnessen P, Engvig A, Grydeland H, Tamnes CK, Ostby Y, Fjell AM, 2010 Life-span changes of the human brain white matter: diffusion tensor imaging (DTI) and volumetry. Cerebral cortex (New York, N.Y. : 1991) 20(9), 2055–2068.

Yeatman JD, Wandell BA, Mezer AA, 2014 Lifespan maturation and degeneration of human brain white matter. Nature communications 5, 4932–4932.

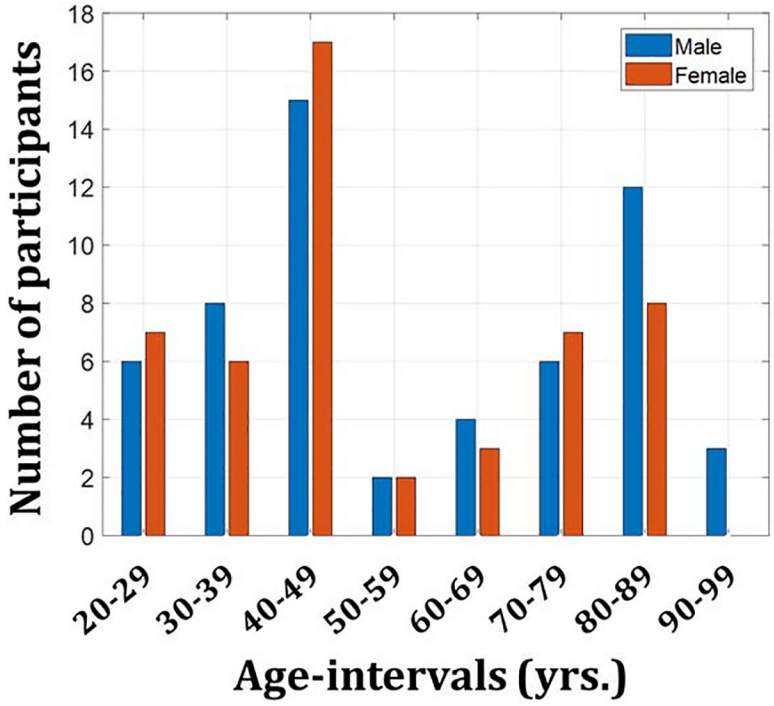

Figure 1.
Number of participants per age-decade and sex within the study cohort.

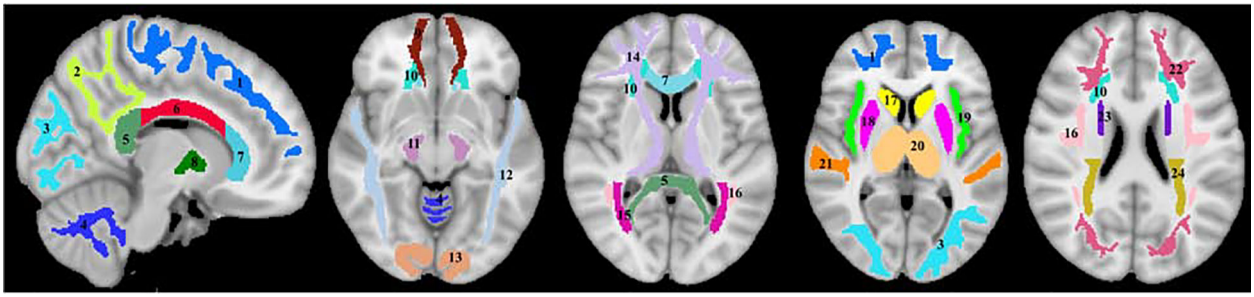

Figure 2.

Visualization of the white matter and deep gray matter ROIs used in our analysis. 1) Frontal lobes, 2) Parietal lobes, 3) Occipital lobes, 4) Cerebellum, 5) Splenium of corpus callosum, 6) Body of corpus callosum, 7) Genu of corpus callosum, 8) Internal capsule, 9) Forceps minor, 10) Interior corona radiata, 11) Cerebral peduncle, 12) Inferior longitudinal fasciculus, 13) Forceps major, 14) Anterior thalamic radiation, 15) Posterior thalamic radiation, 16) Superior longitudinal fasciculus, 17) Caudate, 18) Putamen, 19) Insula, 20) Thalamus, 21) Temporal lobes, 22) Inferior fronto-occipital fasciculus, 23) Superior fronto-occipital fasciculus, and 24) Posterior corona radiata.

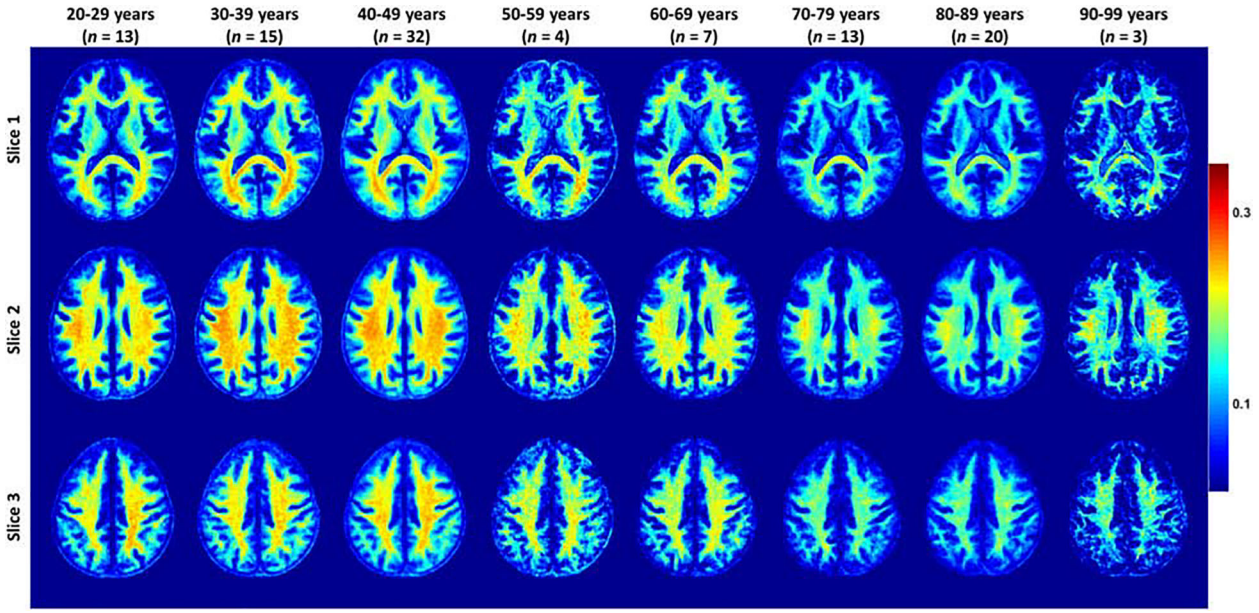

Figure 3.

Myelin water fraction (MWF) represented as averaged participant maps calculated over 10-year intervals. Results are shown for three representative slices. Visual inspection of MWF maps shows an increase in MWF values from early age until middle age, that is, 40–49 year, followed by a more rapid decrease in several brain regions. This suggests progressive myelination continuing into middle age followed by a decline in myelin content at older ages.

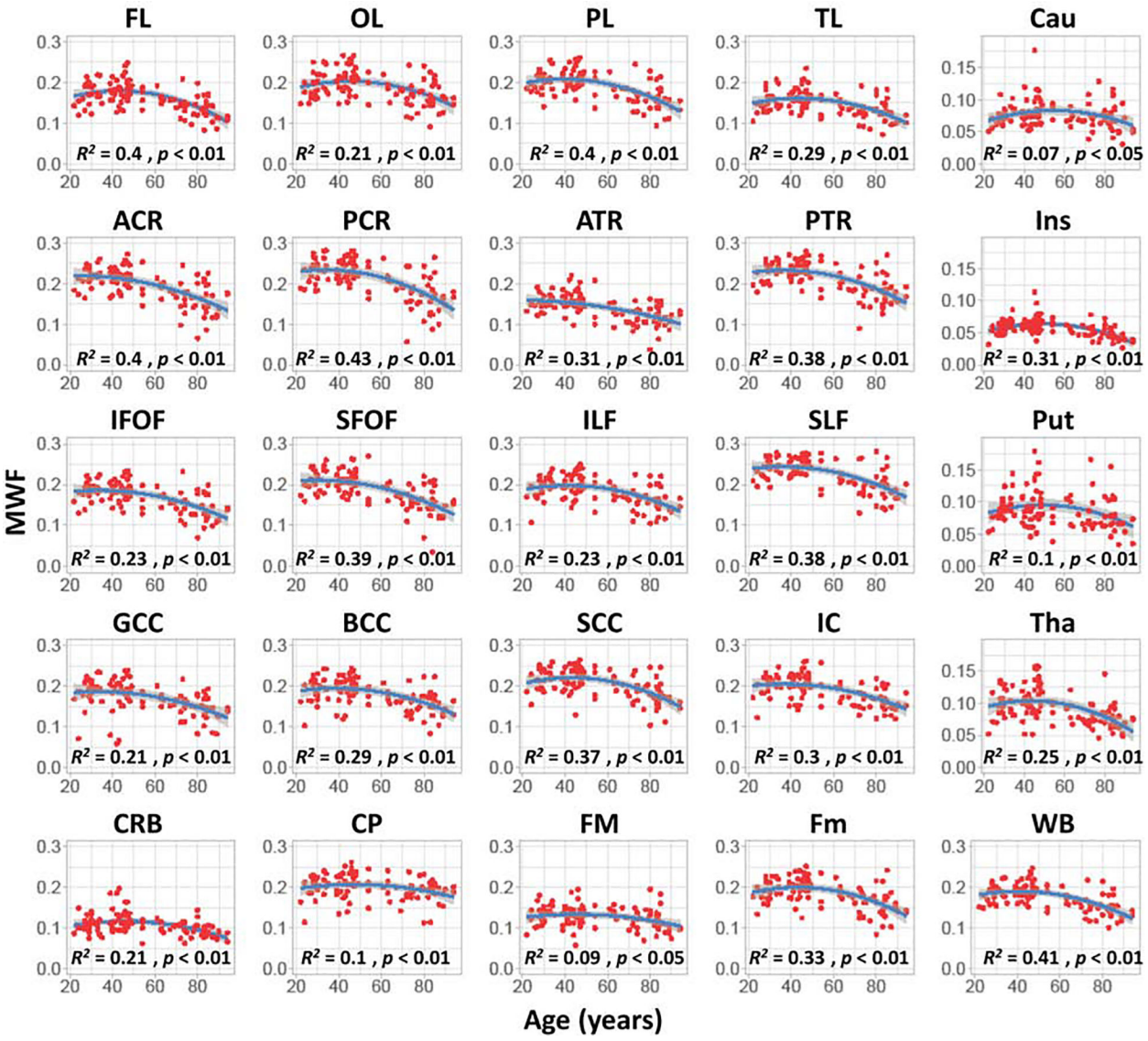

Figure 4.

Regional myelin water fraction (MWF) trajectories as a function of age. For each ROI, the coefficient of determination, R^2, and the significance of the linear regression model, p, are reported. Gray areas indicate 95% confidence intervals. All regions investigated show an inverted U-shaped trend of MWF with age, but with differences in detail between regions in MWF trajectories with age. WB: whole brain white matter, FL: frontal lobes, PL: parietal lobes, OL: occipital lobes, TB: temporal lobes, CRB: cerebellum, SCC: splenium of corpus callosum, BCC: body of corpus callosum, GCC: genu of corpus callosum, IC: internal capsule, ACR: anterior corona radiata, PCR: posterior corona radiata, CP: cerebral peduncle, PTR: posterior thalamic radiation, ATR: anterior thalamic radiation, SFOF: superior fronto-occipital fasciculus, IFOF: inferior fronto-occipital fasciculus, SLF: superior longitudinal fasciculus, ILF: inferior longitudinal fasciculus, FM: forceps major, Fm: forceps minor, Ins: insula, Cau: caudate, Put: putamen, Tha: thalamus, MWF: myelin water fraction.

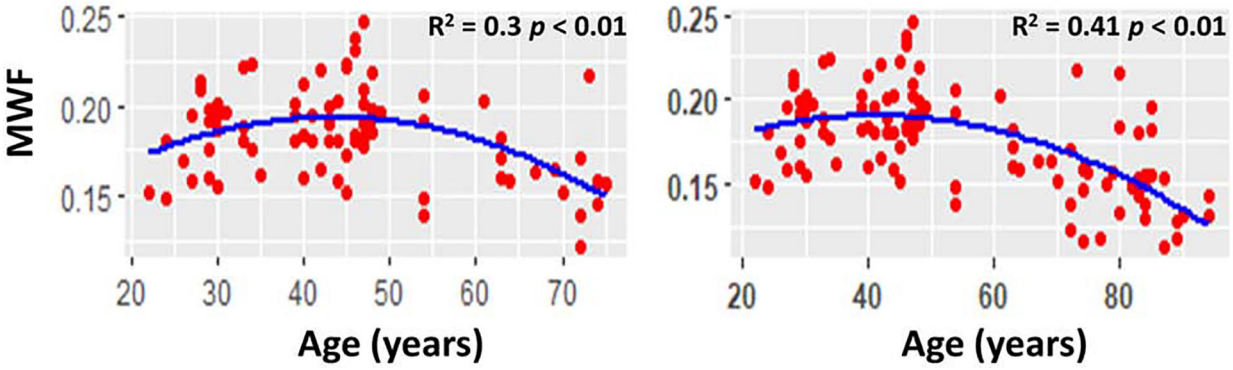

Figure 5.

Myelin water fraction (MWF) as a function of age for white matter throughout the entire brain. Left panel: results obtained on a subset of participants covering a similar age range as in a previous study (Arshad, Stanley, and Raz 2016), that is, excluding participants over age 75. Right panel: results obtained from our full dataset, that is, incorporating all participants. The coefficient of determination, R^2, and the significance of the linear regression model, p, are reported. It is readily seen that exclusion of the oldest participants, that is, over 75 years, shifts the apparent age of maximum myelination derived from the fit toward late ages; this partially explains the discrepancy reported in the literature regarding the apparent age of maximum myelination (Fjell et al. 2010). Of note, a similar effect was observed in most ROIs.

Table 1.

Study group characteristics stratified by sex (mean (standard deviation values))

	Men	Women	*p*
Number	58	48	NA
Age (years)	56.7 (22.5)	53.4 (20)	0.41
MMSE	28.3 (1.7)	28.9 (1.4)	0.051
Education (years)	15.6 (2.9)	16.6 (2.4)	0.054

MMSE: Mini Mental State Examination. The mean and standard deviation (SD) MMSE values were calculated over 101 participants as the MMSE scores of five participants (3 males) were not available, while the mean and SD values of the education years were calculated over 102 participants as the education years of four participants (2 females) were not available. Although the difference in MMSE and educational level between men and women did not formally reach statistical significance, we nevertheless performed analyses correcting for both of these covariates; results were virtually unchanged from those presented in Table 2.

Table 2.

Significance of regression terms in the linear regression, year of apparent maximum myelination, runs test of randomness, and ANOVA from MWF values across age-intervals.

	Age		Age^2		Year of maximum MWF	RTR	ANOVA	
	p	*F*	*p*	*F*		*p*	*p*	*F*
WB	**< 0.01**	50.4	**< 0.01**	10.2	39.7	> 0.1	**< 0.01**	9.9
FL	**< 0.01**	46.6	**< 0.01**	12.8	42.3	> 0.1	**< 0.01**	8.7
OL	**< 0.01**	16.7	**< 0.01**	6.6	45.9	> 0.1	**< 0.01**	5.3
PL	**< 0.01**	52.1	**< 0.01**	9.0	38.2	> 0.1	**< 0.01**	9.6
TL	**< 0.01**	29.2	**< 0.01**	8.8	43.0	> 0.1	**< 0.01**	7.0
CRB	**< 0.01**	19.6	**< 0.01**	7.9	45.1	> 0.1	**< 0.01**	4.5
BCC	**< 0.01**	29.4	**< 0.05**	4.4	36.7	> 0.1	**< 0.01**	6.1
GCC	**< 0.01**	26.2	> 0.1	2.2	NA	> 0.1	**< 0.01**	4.2
SCC	**< 0.01**	36.4	**< 0.01**	9.6	42.0	> 0.1	**< 0.01**	7.1
IC	**< 0.01**	35.4	**< 0.05**	4.2	33.9	> 0.1	**< 0.01**	6.7
ACR	**< 0.01**	60.3	**< 0.05**	3.4	23.3	> 0.1	**< 0.01**	10.4
PCR	**< 0.01**	60.5	**< 0.05**	6.6	33.2	**< 0.05**	**< 0.01**	11.1
CP	**< 0.05**	5.7	> 0.1	1.2	NA	> 0.1	> 0.1	1.4
PTR	**< 0.01**	52.3	**< 0.01**	7.1	35.7	> 0.1	**< 0.01**	11.8
ATR	**< 0.01**	43.7	> 0.1	1.7	NA	**< 0.05**	**< 0.01**	8.7
SFOF	**< 0.01**	60.8	**< 0.05**	4.7	28.5	> 0.1	**< 0.01**	10.2
IFOF	**< 0.01**	23.4	**< 0.05**	3.5	36.7	> 0.1	**< 0.01**	4.2
SLF	**< 0.01**	50.9	**< 0.01**	6.5	35.0	> 0.1	**< 0.01**	9.7
ILF	**< 0.01**	21.2	**< 0.01**	5.3	41.5	> 0.05	**< 0.01**	4.8
FM	> 0.05	3.1	**< 0.05**	4.0	50.7	**< 0.05**	> 0.05	1.9
Fm	**< 0.01**	32.3	**< 0.01**	9.6	42.9	**< 0.05**	**< 0.01**	7.4
Cau	> 0.1	0.9	**< 0.05**	6.0	54.7	> 0.1	> 0.1	1.4
Ins	**< 0.01**	24.4	**< 0.01**	21.1	49.2	> 0.1	**< 0.01**	6.1
Put	**< 0.01**	7.0	**< 0.05**	4.9	48.1	> 0.1	**< 0.05**	2.2
Tha	**< 0.01**	25.5	**< 0.01**	7.9	43.2	> 0.1	**< 0.01**	6.3

WB: whole brain white matter, FL: frontal lobes, PL: parietal lobes, OL: occipital lobes, TB: temporal lobes, CRB: cerebellum, SCC: splenium of corpus callosum, BCC: body of corpus callosum, GCC: genu of corpus callosum, IC: internal capsule, ACR: anterior corona radiata, PCR: posterior corona radiata, CP: cerebral peduncle, PTR: posterior thalamic radiation, ATR: anterior thalamic radiation, SFOF: superior fronto-occipital fasciculus, IFOF: inferior fronto-occipital fasciculus, SLF: superior longitudinal fasciculus, ILF: inferior longitudinal fasciculus, FM: forceps major, Fm: forceps minor, Ins: insula, Cau: caudate, Put: putamen, Tha: thalamus. RTR: run test of randomness for the model incorporating a quadratic age term, MWF: myelin water fraction. NA indicates not applicable for a non-significant Age^2 term. Bold indicates significance. Besides the ANOVA results, all p-values presented are obtained after FDR correction.